Collective structure of the $N = 40$ isotones

L. Gaudefroy,[1] A. Obertelli,[2] S. Péru,[1] N. Pillet,[1] S. Hilaire,[1] J.-P. Delaroche,[1] M. Girod,[1] and J. Libert[3]
[1]*CEA, DAM, DIF, F-91297 Arpajon, France*
[2]*CEA-Saclay, DSM/IRFU/SPhN 91191 Gif-sur-Yvette, France*
[3]*Institut de Physique Nucléaire, IN2P3-CNRS, F-91406 Orsay-Campus, France*
(Received 6 October 2009; revised manuscript received 18 November 2009; published 16 December 2009)

The structure of even-even $N = 40$ isotones is studied from drip line to drip line through the systematic investigation of their quadrupole modes of excitation. Calculations are performed within the Hartree-Fock-Bogoliubov approach using the Gogny D1S effective interaction. Where relevant, these calculations are extended beyond mean field within a generator-coordinate-based method. An overall good agreement with available experimental data is reported, showing that collectivity increases from the neutron to the proton drip line. Whereas ^{60}Ca and ^{68}Ni display a calculated spherical shape in their ground states, all other isotones show a prolate-deformed ground-state band and a quasi-γ band. Coexistence features are predicted in the neutron-deficient $N = 40$ isotones above ^{74}Se.

DOI: 10.1103/PhysRevC.80.064313 PACS number(s): 21.60.Ev, 21.60.Jz, 21.10.Re, 27.50.+e

I. INTRODUCTION

In the last decades experimental studies of the structure of exotic nuclei have changed the accepted idea of robust shell closures built from our knowledge established on stable nuclei. The vanishing of the $N = 20$ shell closure in the vicinity of ^{32}Mg is one of the well-established examples of such strong evolution of nuclear structure [1]. New shell closures may also arise away from the stability line. In that context, the question of $N = 40$ as a magic number in exotic nuclei was previously raised [2]. In a simplistic shell-model description, $N = 40$ is a subshell closure since neutrons fill up the fp shell, with the $1g_{9/2}$ orbital remaining empty. It has been argued that enhanced diffuseness of the nuclear potential in very neutron-rich nuclei can lessen the spin-orbit interaction giving a magic feature to $N = 40$, as observed in atomic physics [3]. However, up to now, evidence for such an effect has never been reported in nuclear physics.

Along the Ni isotopes, presenting a magic number of protons, a relatively large excitation energy of the first 2^+ excited state is observed at $N = 40$. Bernas and co-workers pointed out the "quasi magic" behavior of the nucleus ^{68}Ni [2]. Indeed, the first excited state in ^{68}Ni is a 0^+ state about 300 keV below the 2^+_1 level lying at 2.03 MeV. The occurrence of a 0^+ state as the first excited state in even-even nuclei can be interpreted as evidence for shell closure, as in ^{16}O and ^{40}Ca. It can also provide evidence for shape coexistence as in ^{44}S [4], ^{72}Kr [5], or ^{188}Pb [6]. Apparently, supporting the magical feature of $N = 40$ is the low-reduced transition probability $B(E2; 2^+_1 \rightarrow 0^+_1)$ reported for ^{68}Ni [7]. However, a shell-model-based interpretation of the structure of this nucleus revealed that the size of the $N = 40$ gap did not preclude pairing correlations to develop [7]. Similar conclusions were also reached in shell-model Monte Carlo and quasiparticle random-phase-approximation calculations [8]. Further, toward the neutron drip line, spectroscopic information extend up to $^{66}_{26}$Fe. Recently, deep-inelastic collisions [9] and two-proton knockout reactions [10] were used to perform in-beam γ spectroscopy of this nucleus. From these recent studies and earlier β-decay experiments in the vicinity of $N = 40$ [11,12], deformation was claimed to occur in this mass region and the strong influence of the $\nu g_{9/2}$ orbit on the structure of these nuclei was pointed out. More recently, Tarasov and co-workers suggested a new island of inversion in the region of $^{62}_{22}$Ti from systematics of production cross sections [13].

On the neutron deficient side, the nuclei in the mass region of interest are known to exhibit complex shape features far from closed-shell nuclei characteristics as, for example, in the light Kr and Se isotopes [14,15]. Tetrahedral deformation can also be favored in this region [16].

The present article aims at characterizing the structure of $N = 40$ isotones from drip line to drip line by studying their low-lying quadrupole spectroscopic properties. With this aim in mind, the generator coordinate method within the Gaussian overlap approximation was applied to perform configuration mixing of Hartree-Fock-Bogoliubov (HFB) states. This approach, here labeled five-dimensional collective Hamiltonian (5DCH), treats explicitly all quadrupole degrees of freedom (i.e., two for vibration and three for rotation) [17–19]. Our 5DCH model has already demonstrated its reliability for the description of nuclear properties over the nuclear chart [19–23] using the D1S Gogny effective interaction [24,25]. An abundant literature is currently devoted to the inclusion of a tensor term in phenomenological effective interactions. When it is fitted in a consistent way with the other interaction components, small effects are predicted at the mean-field level [26]. Beyond mean field, modifications of calculated spectroscopy due to the tensor interaction cannot be ruled out. However, the absence of an explicit tensor term in the D1S Gogny interaction is not expected to affect notably the present description of quadrupole collective low-lying states and electric-reduced transition probabilities.

The article is organized as follows. In Sec. II, we discuss the evolution of the spherical neutron and proton shell gaps around the Fermi levels as well as the static axial and triaxial deformation properties predicted for $N = 40$ isotones at a pure mean-field level. Reported results were obtained

from constrained HFB calculations [18]. In Sec. III the low-lying spectroscopy of the studied isotones calculated within the 5DCH approach [17,19] is presented and compared to available experimental data. In particular, Sec. III A and Sec. III B discuss the systematic occurrence of dynamical deformations for the ground-state and excited bands, respectively. Section III C reports on shape coexistence features in the heaviest $N = 40$ isotones. A discussion devoted to the spectroscopic properties of the nuclei ^{68}Ni and ^{60}Ca is reported in Sec. III D. Summary and conclusions are given in Sec. IV.

II. MEAN-FIELD DESCRIPTION

In this study calculations are performed within triaxial symmetries. The results will be introduced step by step, beginning with the peculiar case of imposed spherical symmetry to discuss the evolution of the gap for the $N = 40$ even-even isotones. Next, results for constrained HFB calculations, where axial symmetry is imposed, will be presented to investigate the nature of the $N = 40$ subshell (i.e., the intrinsic deformation of the ground state). Then the influence of triaxial degree of freedom will be briefly discussed.

In this article we use the dimensionless axial and triaxial deformation β and γ parameters [20] that are expressed in terms of the mean values q_{20} and q_{22} of the quadrupole mass operators $\hat{Q}_{20}$ and $\hat{Q}_{22}$, respectively,

$$\beta = \sqrt{\frac{\pi}{5}}\frac{\sqrt{q_{20}^2 + 3q_{22}^2}}{\langle r^2\rangle_A} \quad \text{and} \quad \gamma = \arctan\frac{\sqrt{3}q_{22}}{q_{20}},$$

where $\langle r^2\rangle_A$ is the mean-square radius of a mass-A nucleus [17]. From a technical point of view, HFB equations are solved in a triaxial harmonic oscillator (HO) basis including 11 major shells. We checked that this basis size provides well-converged results for all $N = 40$ isotones at all deformations of present interest. Technical details on the HO basis parameters are provided in the Appendix.

At the mean-field level, the $N = 40$ even-even nuclei that are stable against a two-particle emission range from $Z = 18$ (^{58}Ar) to $Z = 42$ (^{82}Mo). Here we approximate the neutron (proton) drip-line nucleus as the last one for which the two-neutron (two-proton) separation energy is positive, as discussed in more detail in Ref. [27].

The spherical neutron HFB single-particle energies (SPE's) of $N = 40$ isotones, extracted in the canonical basis, are displayed in Fig. 1. It is worth mentioning that, for both proton and neutron SPE's, the present results obtained with the Gogny D1S effective interaction do not differ much from those obtained with well-adopted Skyrme interactions (see e.g., Refs. [28–30]). The $N = 40$ spherical shell gap between the fp shell and the $g_{9/2}$ orbit is found to be rather constant, around 3.9 MeV from $^{58}_{18}$Ar to $^{82}_{42}$Mo. This value, smaller than that found for the $N = 20$ and $N = 28$ shell gaps (4.5 MeV) reported in Ref. [21], is the first indication that neutron pairing correlations develop in $N = 40$ isotones, at least at sphericity. While filling up the proton fp shell along the $N = 40$ isotonic chain, the $\nu 1f_{5/2}$ orbit drops in energy more steeply than do the $\nu 2p$ orbits. Therefore, the $1f_{5/2}$ orbit, predicted to lie above

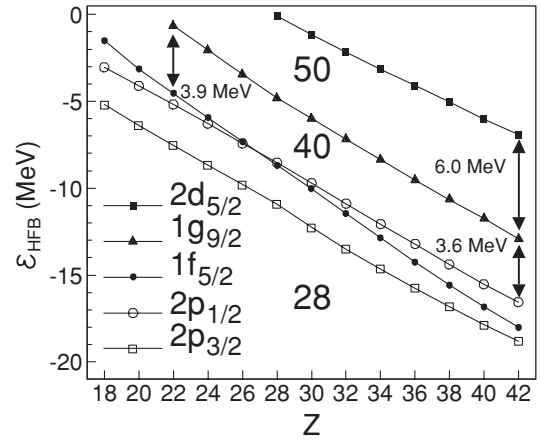

FIG. 1. Spherical neutron HFB single-particle energies for even-even $N = 40$ nuclei.

the $2p_{1/2}$ one for $Z = 20$–24, crosses this latter one at $Z = 26$ and lies between the two $\nu 2p$ spin-orbit partners in nuclei with $Z > 28$.

The relative energy spacings between proton SPE's (not shown here) do not evolve much in the range of studied nuclei, irrespective of the occupation numbers of the proton orbits. The $d_{3/2}$–$f_{7/2}$ gap, the so-called $Z = 20$ gap, amounts to almost 8 MeV. The energy gap above the $f_{7/2}$ orbit ($Z = 28$) is of 5.5 MeV and the other fp-shell orbits, $f_{5/2}$, $p_{3/2}$, and $p_{1/2}$, lie within around 3 MeV. The energy spacing between fp and gd shells ($Z = 40$) is approximately 4 MeV. Data from the pick-up and stripping reactions needed for a comparison with calculations are very scarce for $N = 40$ isotones, precluding the extraction of reliable experimental SPE's. If any, future comparisons need to be performed with caution since beyond-mean-field correlations are expected to compress single-particle spectra.

The evolution of total energy as a function of the axial deformation parameter β is displayed in Fig. 2 for all even-even $N = 40$ isotones. The curves are the result of constrained HFB calculations. Most of the isotones present a spherical minimum except ^{72}Ge and ^{74}Se; both show a rather flat potential energy curve for β values ranging from -0.3 to 0.1, the minimum of which is found for an oblate deformation parameter $\beta \simeq -0.2$. A clear feature is the existence of a prolate shell effect (around $\beta = 0.5$), present in each isotone that produces a secondary minimum for Cr, Fe, Ni, Kr, Sr, Zr, and Mo. Even if less pronounced, shoulders are also present at oblate deformation ($\beta \simeq -0.5$) in most of the potential energy curves presented in Fig. 2. The general features of the potential energy curves are related to the existence of proton and/or neutron shell effects in the single-particle spectra as functions of the axial deformation shown in Fig. 3 for $^{76}_{36}$Kr. As for the SPE's, the deformed single-particle spectra in Fig. 3 are quite similar to those obtained with Skyrme interactions [29].

Pairing energy is very sensitive to shell effects. This quantity is displayed in Fig. 4 as a function of β, both for protons and neutrons. As a general rule, a decrease (increase) of the level density around the Fermi level is always accompanied by an decrease (increase) of pairing energy. As

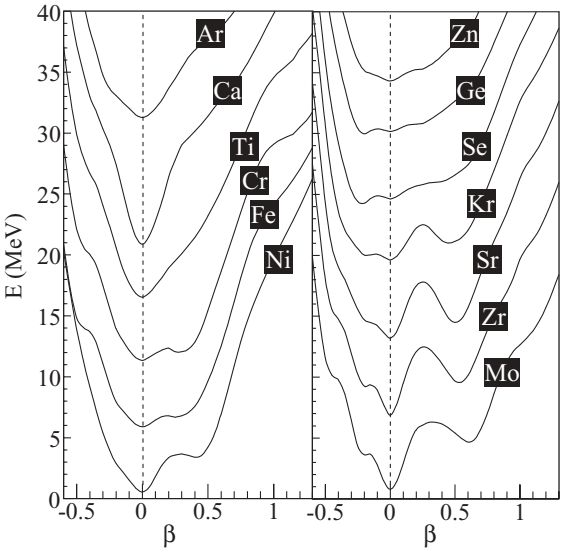

FIG. 2. Potential energy curves for the $N = 40$ isotones as functions of the axial deformation parameter β. The curves, labeled with chemical symbols, are offset by some arbitrary absolute energy for ease of comparison.

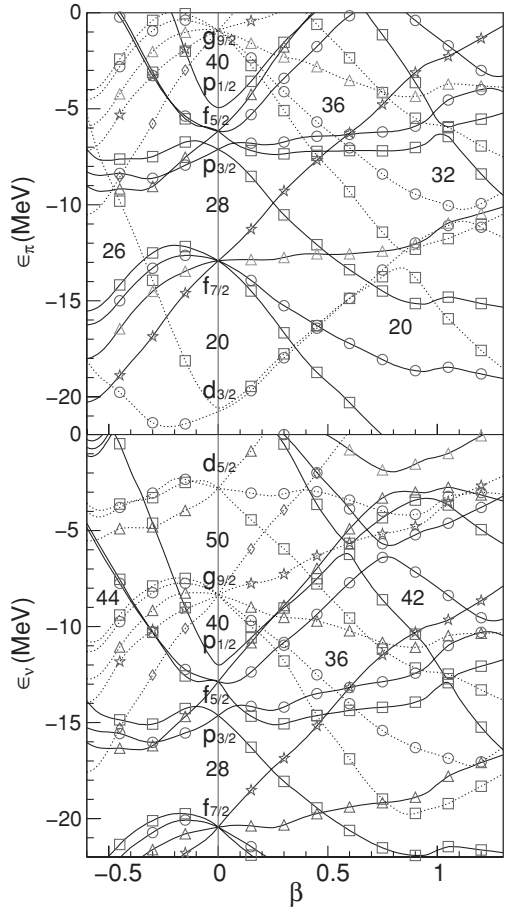

FIG. 3. Sequence of proton (top) and neutron (bottom) single-particle levels as functions of the axial deformation parameter β in $^{76}_{36}$Kr. Dashed (solid) lines represent positive (negative) parity orbits. Each orbit is characterized by: (i) its spherical quantum numbers, reported at $\beta = 0$, and (ii) its K quantum number (projection of the angular momentum on the z symmetry axis) as follows: square for $K = 1/2$, circle for $K = 3/2$, triangle for $K = 5/2$, star for $K = 7/2$, and diamond for $K = 9/2$.

seen from Fig. 4, the neutron pairing energy curves are found to be rather similar from $Z = 18$ to $Z = 42$. This reflects the similarity in the sequence of individual neutron levels with axial deformation from one isotone to the other. For each isotone, the spherical $N = 40$ shell gap is found to be of a similar magnitude for β values in the vicinity of $\beta = 0$ (see Fig. 3). In the vicinity of $\beta = 0.5$, the neutron level density around the Fermi level is systematically low, accounting for the minima observed in the neutron pairing energies shown in Fig. 4. A slight decrease in the neutron level density is found at oblate deformations (around $\beta = -0.2$ and -0.5). From Fig. 3, one sees that, to correctly define the Fermi level in $N = 40$ isotones, the fp, $g_{9/2}$, and $d_{5/2}$ shells have to be considered. Each of the aforementioned shell effects has its counterpart (i.e., a minimum) in the neutron pairing energy curves displayed in Fig. 4.

Contrary to the neutron case, the proton pairing energy curves vary drastically along the $N = 40$ chain, reflecting strong proton (deformed or not) shell effects encountered from $Z = 18$ to $Z = 42$. Depending on the nucleus, and hence on the shell structure around the Fermi level, the proton pairing energy presents deep minima (that can reach zero) for various β values. For example, the large $Z = 20$ and $Z = 28$ spherical gaps (seen in Fig. 3) preclude proton pairing correlations from taking place in the corresponding isotones at $\beta = 0$. However, for none of the other isotones does proton pairing energy vanish around $\beta = 0$. Pairing energy vanishes at extreme oblate deformation ($\beta = -0.5$) for $^{66}_{26}$Fe due to a large deformed-proton shell gap. In $^{72}_{32}$Ge, proton pairing is null at very large prolate deformation ($\beta = 0.9$), as it is for $^{60}_{20}$Ca. It is interesting to notice that, from $Z = 30$ to $Z = 34$, proton and neutron pairing energies present "out of phase" variations against deformation in such a way that their sum is rather constant. These features stand at the origin of the flat potential energy curves reported in Fig. 2 for the corresponding isotones. On the contrary, proton and neutron pairing energies for nuclei with $Z \geqslant 36$ present minima in the same prolate region ($\beta \simeq 0.5$), thus favoring the secondary minimum built up in potential energy curves of Fig. 2.

To go further in the analysis of the topology of potential energy and shell effect, the triaxial potential energy surface (PES) of each studied isotone was calculated. Four types of triaxial PES's are found. Figure 5 displays a typical example for each of the four groups: (i) $^{58}_{18}$Ar, $^{60}_{20}$Ca, and $^{62}_{22}$Ti present a rigid triaxial surface centered around sphericity; (ii) $^{64}_{24}$Cr, $^{66}_{26}$Fe, $^{68}_{28}$Ni, and $^{70}_{30}$Zn present similar PES's with a minimum in the spherical region and an extension toward the prolate region; (iii) $^{72}_{32}$Ge and $^{74}_{34}$Se form another group for which minimum in the triaxial plane is broader than for lighter isotones resulting in a rather flat PES where an oblate minimum is found ($\gamma = 60°$); and (iv) The four heaviest $N = 40$ isotones studied here present PES's for which two clear minima are observed, one near the spherical point and the other at large prolate deformation, as shown in Fig. 5 for $^{78}_{38}$Sr. For each group, one

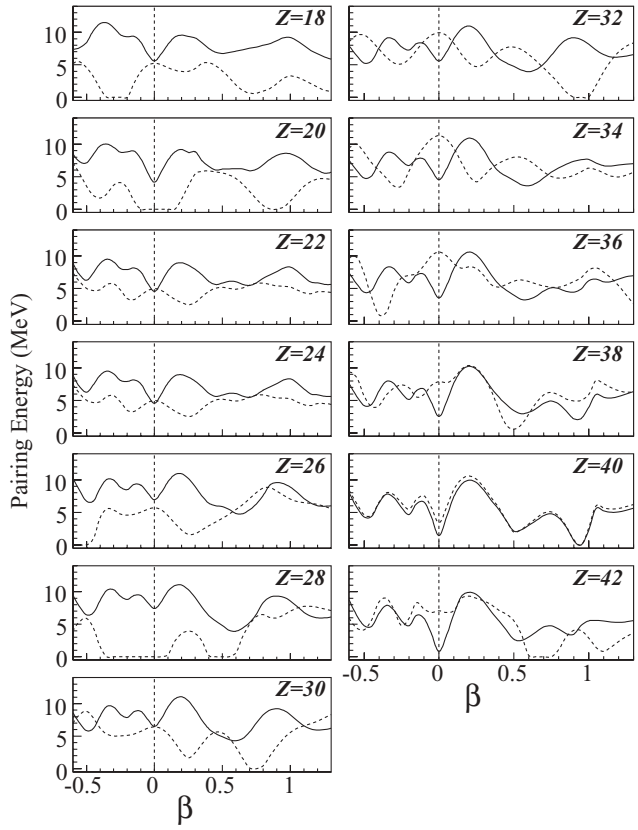

FIG. 4. Proton (dashed lines) and neutron (solid lines) pairing energy curves as functions of the axial deformation parameter β. Each panel represents one of the $N = 40$ isotones under study, labeled by its Z value.

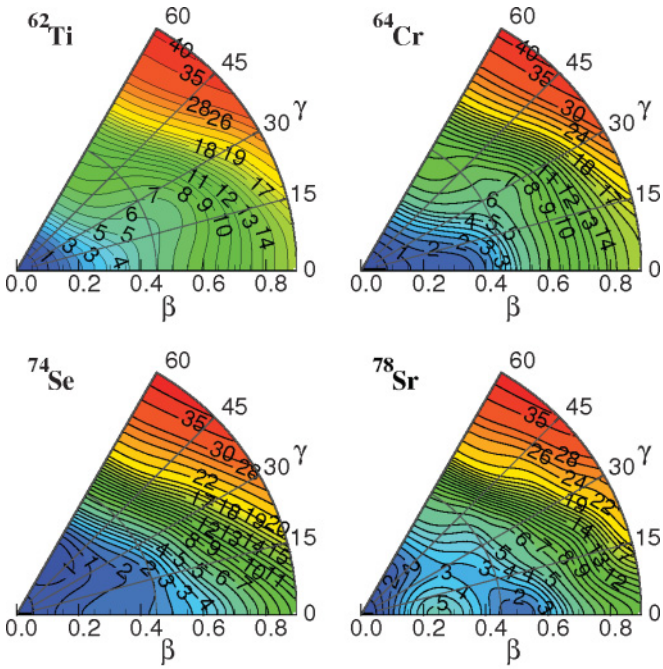

FIG. 5. (Color online) Triaxial potential energy surfaces (in MeV) for $^{62}_{22}$Ti, $^{64}_{24}$Cr, $^{74}_{34}$Se, and $^{78}_{38}$Sr.

clearly recognizes the various axial minima discussed from Fig. 2. For all isotones, the PES's do not show triaxial minima that modified the conclusions obtained from the discussion of axial results.

To summarize all these mean-field results, at the spherical point the $N = 40$ shell gap is constant and amounts to about 3.9 MeV, a value not strong enough to hinder neutron pairing correlations. On the one hand, the spherical configuration is favored at the mean-field level for all but two $N = 40$ isotones ($^{72}_{32}$Ge and $^{74}_{34}$Se). On the other hand, both proton and neutron shell effects produce "perturbations" in the studied potential energy curves leading, for heavier isotones, to a deep secondary minimum at prolate deformation. These features indicate the need of a beyond-mean-field treatment consisting of deformed configuration mixing to achieve a more definite description of the isotones under study.

III. QUADRUPOLE COLLECTIVE SPECTROSCOPY

In this section the low-lying spectroscopy of $N = 40$ isotones is discussed to assess their collectivity. To perform this analysis the 5DCH approach [17,19] that accounts for *quadrupole* correlations was adopted. Within this approach, the calculated states have good angular momentum J and parity $\pi = +$. For later convenience it is mentioned that the wave functions of the collective states decompose into K components, where K is the projection of angular momentum onto the z axis in the intrinsic system.

The reader should note that the present approach deals only with quadrupole correlations. The occurrence of negative parity states, and especially 3^- states, will not be addressed. It is to be mentioned that such states have been observed in numerous $N = 40$ isotones, at an excitation energy in the 2.5–3 MeV range, similar to that for the positive parity levels of present interest [31]. Whenever possible, comparison with experimental data is presented. Data are taken from the Brookhaven database [32], except when explicitly mentioned.

Reported results concern all $N = 40$ isotones except $^{58}_{18}$Ar, $^{60}_{20}$Ca, and $^{68}_{28}$Ni. Because of proton magic numbers, the present 5DCH treatment may not be well suited for the two last isotones. Concerning $^{58}_{18}$Ar, the unoccupied levels (in the Hartree-Fock sense) are unbound at the spherical point (see Fig. 1). A similar observation is also made whatever the values of β are, except for large oblate ones. As the credit due to our beyond-mean-field treatment for this nucleus will be disputable, $^{58}_{18}$Ar is excluded from the following discussion. Finally, all spectroscopic results presented in the following are summarized in Table I.

A. Ground-state band

Available experimental data concerning the excitation energy of the 2^+_1 states in $N = 40$ isotones are reported in Fig. 6(a). For each isotone, this state lies at a rather low excitation energy (below 1 MeV, except in ^{68}Ni), the first indication for a somewhat collective character. Associated with these excitation energies, Fig. 6(b) displays the available experimental reduced transition probabilities [$B(E2)$'s]

TABLE I. Predicted excitation energies $E(J^\pi)$ in MeV; spectroscopic quadrupole moments $Q(J^\pi)$ in e fm^2; reduced transition probabilities $B(E2; J_i \to J_f)$ in e^2 fm^4; and percentages of the $K = 0$ component for the 2_2^+ and 2_3^+ states calculated within the present 5DCH approach for the studied $N = 40$ isotones.

Isotone	$^{62}_{22}$Ti	$^{64}_{24}$Cr	$^{66}_{26}$Fe	$^{70}_{30}$Zn	$^{72}_{32}$Ge	$^{74}_{34}$Se	$^{76}_{36}$Kr	$^{78}_{38}$Sr	$^{80}_{40}$Zr	$^{82}_{42}$Mo
$E(2_1^+)$	1.145	0.822	0.851	0.928	0.747	0.668	0.520	0.332	0.343	0.488
$E(4_1^+)$	2.165	1.794	1.892	2.036	1.740	1.483	1.133	0.824	0.847	1.077
$E(6_1^+)$	3.331	3.024	3.200	3.362	2.940	2.449	1.933	1.528	1.561	1.825
$E(2_2^+)$	2.313	2.448	2.306	1.965	1.498	1.274	1.077	1.050	0.940	0.954
$E(3_1^+)$	2.813	3.098	3.193	2.923	2.329	2.039	1.753	1.565	1.370	1.430
$E(4_2^+)$	3.224	3.511	3.554	3.248	2.650	2.201	1.888	1.758	1.606	1.671
$E(5_1^+)$	3.751	4.171	4.442	4.252	3.545	2.986	2.555	2.296	2.079	2.168
$E(6_2^+)$	4.355	4.705	4.973	4.684	3.992	3.349	2.837	2.597	2.417	2.516
$E(0_2^+)$	1.805	2.042	1.987	2.050	1.800	1.258	0.861	0.759	0.829	0.882
$Q(2_1^+)$	−28	−34	−34	−24	−13	−17	−54	−86	−85	−53
$Q(4_1^+)$	−42	−48	−49	−42	−33	−54	−92	−116	−115	−95
$Q(6_1^+)$	−45	−54	−57	−57	−52	−75	−110	−130	−129	−116
$Q(2_2^+)$	23	28	22	15	2[a]	−5[a]	23	58	60	24
$Q(2_3^+)$							−15[a]	−39	−72	−40
$K = 0\,(2_2^+)$	12	10	16	19	28	35	25	13	10	22
$K = 0\,(2_3^+)$							64	73	84	75
$B(E2; 2_1^+ \to 0_1^+)$	199	303	346	441	629	813	1145	1824	1982	1557
$B(E2; 2_2^+ \to 0_1^+)$	7	12	11	4	1	1	14	51	44	6
$B(E2; 2_2^+ \to 2_1^+)$	253	212	308	655	1043	1450	1450	830	1139	2221
$B(E2; 0_2^+ \to 2_1^+)$							2869	2459	2694	3493
$B(E2; 2_3^+ \to 0_2^+)$							875	908	1479	1807

[a]The sign for this quadrupole moment should be considered with caution because of the strong mixing between different K components in the wave function of the state.

measured for the $2_1^+ \to 0_1^+$ transition. The important increase of the $B(E2)$'s with Z clearly reflects the growth in collectivity toward the proton drip line. The results of present 5DCH calculations for the aforementioned observables are also reported in Fig. 6 for comparison. A very good agreement between experimental data and calculations is found for both excitation energies and reduced transition probabilities. In $N = 40$ isotones, correlations are calculated to be maximum in the $N = Z$ nucleus $^{80}_{40}$Zr. This last conclusion is in agreement with that from shell-model Monte Carlo calculations along the

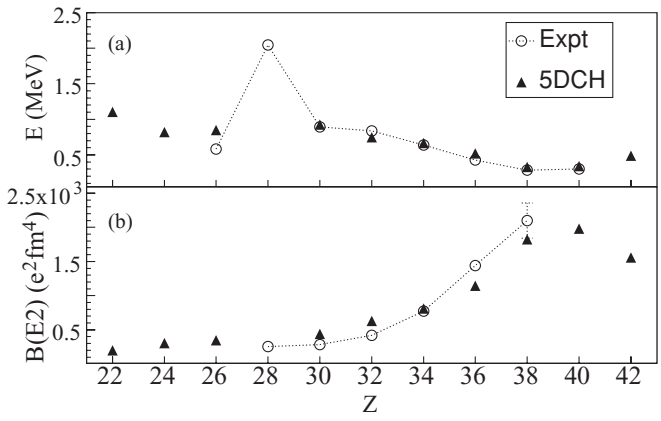

FIG. 6. (a) Excitation energies of the 2_1^+ state of $N = 40$ isotones and (b) reduced transition probabilities $B(E2; 2_1^+ \to 0_1^+)$. 5DCH results are compared to existing experimental data [10,32].

$N = 40$ chain [33]. Collectivity is found to slightly decrease in $^{82}_{42}$Mo, as seen from the increase (decrease) in the 2_1^+ state excitation energy (transition rate) for this nucleus.

One way to gain a deeper insight into the structure of $N = 40$ isotones is by inspecting the yrast-state properties not only restricted to the 2_1^+ states. Taking advantage of the existence of some experimental data for the excitation energy of the 4_1^+ states, we analyze the $R_{42} = E(4_1^+)/E(2_1^+)$ ratio. This latter term is displayed in Fig. 7. The experimental trend to increase from the vibrator value ($R_{42} = 2$) toward the γ-soft value ($R_{42} = 2.5$) with increasing Z is clear. Both $^{78}_{38}$Sr and $^{80}_{40}$Zr present an experimental R_{42} value slightly larger than 2.5, indicating a pronounced collectivity and hence deformation. The systematics of the calculated R_{42} ratio is also reported in Fig. 7. It should first be emphasized that this figure does not do justice to the agreement between theoretical and experimental excitation energies of the 4_1^+ states, which is of a quality similar to that for the 2_1^+ states. Most of the theoretical R_{42} values are close to 2.2. Clearly the calculated R_{42} ratio for $^{62}_{22}$Ti ($R_{42} = 2$) differs from the ones in $^{78}_{38}$Sr and $^{80}_{40}$Zr ($R_{42} = 2.5$). In combination with the PES's presented in Fig. 5, one concludes that $^{62}_{22}$Ti is a rather spherical nucleus. In agreement with the experimental data, $N = 40$ isotones are found to be transitional in nature. They are clearly not expected to behave as rotational nuclei for which $R_{42} = 10/3$, a conclusion that matches the one based on projected shell-model calculations for ^{66}Fe [34].

At this stage of our discussion on the ground-state band properties, it is interesting to include predictions about spectroscopic quadrupole moments, even though experimental data

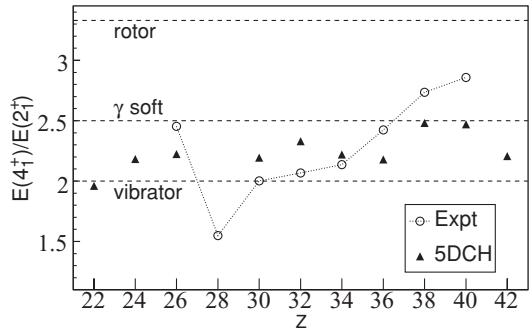

FIG. 7. $E(4_1^+)/E(2_1^+)$ ratio for $N = 40$ isotones. 5DCH predictions are compared to experimental data. Dashed lines indicate vibrational, γ-soft, and axial rotor values for this ratio.

are available only for the 2_1^+ state for the Zn, Ge, Se, Kr, and Sr isotones. Figure 8 displays the experimental data compared with the theoretical ones for the 2_1^+, 4_1^+, and 6_1^+ states. The agreement between the data and calculations is remarkable. The 5DCH calculations foretell a prolate yrast band. Thus, contrary to what can be expected from a pure mean-field treatment (see Fig. 2 and the related discussion), $N = 40$ isotones are calculated to be *dynamically* deformed along the ground-state band within the present 5DCH approach. Deformation and correlations are found to strongly increase while approaching the proton drip line. From Fig. 8 one also sees that the spectroscopic quadrupole moment of the states belonging to the ground-state band increases with increasing spin values. It should be noted that two experimental values are plotted for $^{74}_{34}$Se. They both result from the same χ^2 analysis of the data reported in Ref. [35]. The present calculations strongly support the value of lower magnitude. From the previous discussion, $N = 40$ isotones were shown to be dynamically deformed in their ground state and to display a prolate yrast band, identified up to the 6_1^+ state. In agreement with the studied R_{42} ratios for these isotones, the ground-state band is not a true rotational band and the $N = 40$ isotones are, therefore, labeled as transitional nuclei. Further study of their low-lying spectroscopy, as reported in the following, should bring deeper insight into their characterization.

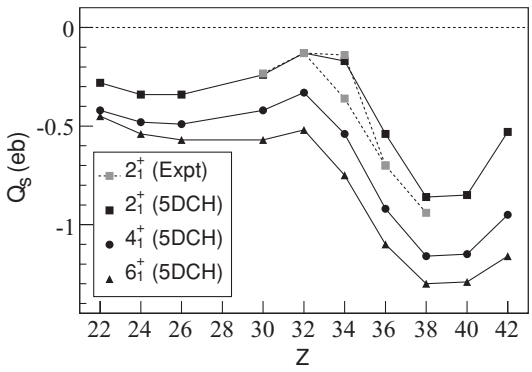

FIG. 8. 5DCH predictions for the spectroscopic quadrupole moments of the 2_1^+, 4_1^+, and 6_1^+ states belonging to the yrast band in $N = 40$ isotones. Available experimental data are reported for comparison.

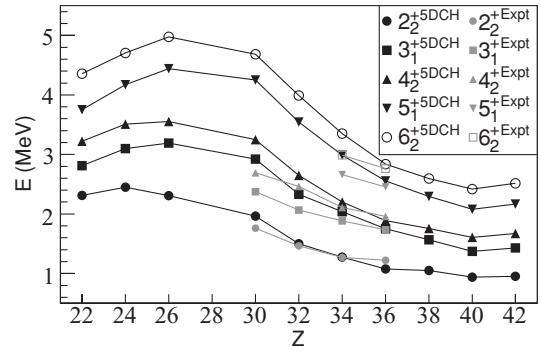

FIG. 9. Excitation energies of the $J \leqslant 6$ states belonging to quasi-γ bands. Available experimental data are reported for comparison.

B. Quasi-γ band

Available experimental data for $N = 40$ isotones reveal a systematic occurrence of low-lying 2_2^+ states associated with typical sequences of $(3_1^+, 4_2^+)$ and $(5_1^+, 6_2^+)$ states, forming vibrational quasi-γ bands. These experimental data, as well as the 5DCH results, are presented in Fig. 9. The agreement between the data and calculations is satisfactory (discrepancy is of 500 keV in the worst case). 5DCH calculations predict the persistence of the quasi-γ band on both neutron-rich and neutron-deficient sides. Further analysis of the 2_2^+ wave functions confirms their prominent $K = 2$ vibrational nature, as inferred from the small amount of $K = 0$ components reported in Table I.

As seen from Fig. 9, beginning with $Z = 22$ one observes a slight increase in the excitation energy of the states up to $Z = 26$. Then, from $Z = 30$ to $Z = 42$, the excitation energy of the states of the bands gradually decreases from about 2 MeV down to 1 MeV for the bandheads. Consistently with the results presented in Sec. III A, this behavior indicates, one more time, the increase of collectivity in $N = 40$ isotones while approaching the proton drip line.

To get further insight into the structure of the quasi-γ band it is instructive to study how the states belonging to that band decay to the 0_1^+ and 2_1^+ ground-state band levels. This provides information on the mixing between both bands. On the experimental side, such data are scarce and mainly restricted to the decay of the 2_2^+ bandhead state we will focus on in the following. This state is mainly observed to decay to the 2_1^+ level with relatively large measured $B(E2)$ values: 1182^{+1748}_{-1182}, 1103(196) and 886(258)e^2 fm^4 in ^{70}Zn, ^{72}Ge, and ^{74}Se, respectively. In ^{76}Kr, the $B(E2)$ value associated with the $2_2^+ \rightarrow 2_1^+$ is significantly lower [$B(E2) = 20(20)$ e^2 fm^4] than for other $N = 40$ isotones [14]. In most of the $N = 40$ isotones, except again in ^{76}Kr, the reduced transition probability associated with the $2_2^+ \rightarrow 0_1^+$ decay is considerably smaller than the previous one toward the 2_1^+ state: 41^{+41}_{-21}, 2.3(4), 15(4), and $67^{+5}_{-4}e^2$ fm^4 in ^{70}Zn, ^{72}Ge, ^{74}Se, and ^{76}Kr, respectively.

These experimental data are to be compared with the results of the present 5DCH calculations, reported in Table I. From a theory/experiment comparison, one sees that the $2_2^+ \rightarrow 2_1^+$

decay rate is rather well accounted for by the present approach (discrepancies smaller than a factor of 2) except in ^{76}Kr, as already discussed in Ref. [14]. On the contrary, the present 5DCH approach strongly underestimates (by about a factor of 10 or more) the $2_2^+ \to 0_1^+$ decay rates. This indicates that the mixing between the ground-state band and the quasi-γ band (or similarly the relative amount of $K = 0$ and $K = 2$ components in the 2_2^+ wave functions) is likely to be slightly underestimated within the present 5DCH approach. The Gaussian overlap approximation and/or the Inglis-Belyaev approximation (used for calculating collective masses) are very likely responsible for these discrepancies.

Finally, as studied for the ground-state band in Sec. III A, the spectroscopic quadrupole moments of the 2_2^+ states were calculated to infer a tendency for the deformation of the quasi-γ band. As seen from Table I, all relevant spectroscopic quadrupole moments for the state of interest are positive and slightly lower in magnitude (a factor of 1.5–2) than those for the first 2^+ states displayed in Fig. 8. This latter observation suggests that the quasi-γ band in $N = 40$ isotones might be viewed as a moderately deformed structure as compared to that for the ground-state band.

C. Coexistence features

The richness and the complex structure of $N = 40$ isotones are also demonstrated by the presence of a low-energy 0_2^+ state experimentally observed in $^{68}_{28}$Ni, $^{70}_{30}$Zn, $^{72}_{32}$Ge, $^{74}_{34}$Se, and $^{76}_{36}$Kr. The special case of $^{68}_{28}$Ni will be discussed in Sec. III D. For other isotones, the low-lying 0_2^+ state is observed below 1 MeV (see Fig. 10). Such low-lying 0_2^+ states might be the signature of shape coexistence. However, early theoretical works [36–39] showed the need for coupling between collective and noncollective degrees of freedom (quasiparticle excitations) to successfully describe these 0_2^+ states in Zn, Ge, and Se isotones. Such coupling modes are not included in the present approach. The situation is quite different in $^{76}_{36}$Kr, for which the occurrence of the low-lying 0_2^+ state has been shown to arise from shape coexistence [14]. The predicted excitation energies of the 0_2^+ states are also reported in Fig. 10 for all studied $N = 40$ isotones. As expected, the present approach thoroughly fails in reproducing the existing 0_2^+ experimental data for Z below $Z = 36$. For this reason, the following discussion is restricted to relevant nuclei with $Z \geqslant 36$. As already seen in Fig. 2, two deep minima are found in the potential energy curves of $N = 40$ isotones with $Z \geqslant 36$. As a consequence, shape coexistence might be favored in these isotones. The predicted occurrence of a 0_2^+ state, lying slightly below 1 MeV, in all heavier $N = 40$ isotones indeed points toward this conclusion.

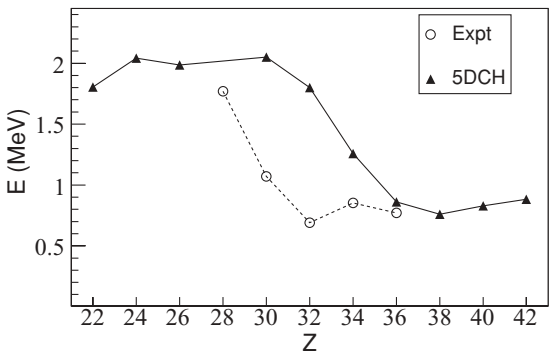

FIG. 10. Predicted excitation energies of the 0_2^+ states in $N = 40$ isotones, compared to available experimental data.

To specify the collectivity of the band built on the 0_2^+ state, the ratio of the calculated reduced transition probabilities $R = B(E2; 2_3^+ \to 0_2^+)/B(E2; 2_1^+ \to 0_1^+)$ was calculated. In the following, this ratio will be used as an indicator for shape coexistence. The values for Kr, Sr, and Zr isotones equal 0.76, 0.50, and 0.75, respectively, and are among the smallest calculated over the nuclear chart [23]. In contrast, the collectivity in $^{82}_{42}$Mo is larger in the excited band than in the ground-state band. It clearly shows that collectivity significantly differs in magnitude between both the ground-state and the $K = 0$ excited bands in the present deformed nuclei, a measure of which also stems from comparing the $Q(2_1^+)$ and $Q(2_3^+)$ values in Table I. Shape coexistence between the prolate ground-state band and the prolate $K = 0$ excited band is thus predicted to occur in all neutron-deficient $N = 40$ isotones above ^{74}Se.

In present isotones it is worth mentioning that the quasi-γ bandhead lies above the $K = 0$ excited bandhead. Therefore, the unique $E2$ decay available to the 0_2^+ state is that toward the 2_1^+ level. The corresponding reduced transition probabilities are reported in Table I for isotones with $Z > 34$.

D. Spherical nuclei: $^{68}_{28}$Ni and $^{60}_{20}$Ca

Finally, based on our results, we comment on the case of the proton magic nuclei $^{60}_{20}$Ca and $^{68}_{28}$Ni, so far left out in previous discussions, starting with $^{68}_{28}$Ni for which experimental data exist. $^{68}_{28}$Ni is the only $N = 40$ isotone presenting an experimental R_{42} value below 2, associated with a relatively large excitation energy of the 2_1^+ state measured slightly above 2 MeV. These are typical features of magic nuclei. Our results on other nuclei, at the mean-field level and beyond mean field, clearly show that $N = 40$ is never a magic number for the following reasons: (i) The neutron pairing energy does not vanish at $\beta = 0$; (ii) Most of the $N = 40$ isotones are dynamically deformed in their ground state; and (iii) Shape coexistence is predicted for some of these isotones. Thus, the low-lying spectroscopic properties of $^{68}_{28}$Ni are interpreted as arising from its magic number of protons combined with a spherical, *but not magic*, neutron shell effect. Other authors reached the same conclusion using different theoretical approaches [8].

Similar properties can be expected for $^{60}_{20}$Ca. Indeed in Fig. 6(a) an increase in the excitation energy of the 2_1^+ state is suggested while going from $Z = 24$ down toward $Z = 20$. More importantly, the potential energy surface for $^{60}_{20}$Ca (see discussion related to Fig. 5) clearly indicates a spherical shape for this nucleus. This is also supported by the results presented in Fig. 4: (i) as for $^{68}_{28}$Ni, the proton pairing energy vanishes at $\beta = 0$ in $^{60}_{20}$Ca; and (ii) Contrary to the prediction for $^{68}_{28}$Ni (and in favor for a spherical shape), the neutron pairing energy is minimum at $\beta = 0$ for $^{60}_{20}$Ca. Thus, from the present

results, a spherical shape is expected to be favored in $^{60}_{20}$Ca. The present conclusion agrees with that obtained within self-consistent Hartree-Fock plus random-phase-approximation calculations using Skyrme interactions [28]. Both interpretations are, however, at variance with the one offered in Ref. [13].

IV. CONCLUSION

The focus of the present article is the study of quadrupole collective properties of the $N = 40$ even-even isotones, investigated using both mean-field (HFB) and beyond-mean-field (5DCH) methods implemented with the D1S Gogny force. In the HFB approach, $N = 40$ never reaches the characteristics of a magic shell closure, even though most of the studied nuclei are calculated as spherical. The $N = 40$ subshell gap, here calculated to be about 3.9 MeV wide, is not large enough to prevent pairing correlations from developing. In the 5DCH approach that includes all quadrupole degrees of freedom, $N = 40$ isotones get dynamically deformed. However, their calculated yrast spectroscopy never matches that of rotors, in agreement with the experimental data. Most of the $N = 40$ nuclei are soft against quadrupole deformation. This softness results in quasi-γ-vibrational bands with head levels calculated in the 1.5–2 MeV excitation energy range. These predictions are also in good agreement with available data. Yrare 0^+ levels were identified from our beyond-mean-field calculations, with energies that do not match experimental data for $Z \leqslant 34$. This result brings confirmation of the complex structure of 0^+_2 excitations in these nuclei and implies that the present theory be extended to include quasiparticle degrees of freedom. The calculated energies of the first yrare 0^+ state significantly drop to below 1 MeV for $Z > 34$ and shape-coexistence is predicted in these neutron-deficient isotones. In the particular case of ^{76}Kr experimental data support our conclusion. Dedicated measurements on ^{78}Sr and ^{80}Zr are welcome to further assess the reliability of present predictions far from stability.

Finally, $^{60}_{20}$Ca and $^{68}_{28}$Ni are singled out since both have a magic number of protons. Our interpretation is that these proton shell closures play a key role in driving $^{60}_{20}$Ca and $^{68}_{28}$Ni toward a spherical shape.

Since $N = 40$ isotones are calculated as soft against quadrupole deformations and display positive and negative parity states at similar excitation energies, the question arises as to whether quadrupole and octupole modes strongly couple each other. To shed light on this issue, which is of broad relevance for nuclear spectroscopy, it will be wise to extend the present mean-field and beyond-mean-field models to a higher number of collective coordinates. Such a prospect is very challenging, but tractable with the advent of powerful computers.

APPENDIX: TRIAXIAL BASIS PARAMETERS

In the present HFB calculations the HO states constituting the basis are chosen following a deformed truncation scheme linked to the (β,γ) parameters

$$\begin{aligned}\left(n_x + \tfrac{1}{2}\right)\hbar\Omega_x + \left(n_y + \tfrac{1}{2}\right)\hbar\Omega_y + \left(n_z + \tfrac{1}{2}\right)\hbar\Omega_z \\ \leqslant (N_0 + 2)\hbar\Omega_0,\end{aligned} \tag{A1}$$

where n_x, n_y, and n_z are the numbers of quanta in the three spacial directions x, y, and z, respectively, and N_0 is the basis size, that is, $N_0 + 1$ is the number of major shells (11 in the present work). Here, Ω_i represents the energy truncation parameter in the i direction. The parameter Ω_0 is defined as $\Omega_0^3 = \Omega_x\Omega_y\Omega_z$.

Thus, inserting the ratios $P = \frac{\hbar\Omega_x}{\hbar\Omega_y}$ and $Q = \frac{\hbar\Omega_x}{\hbar\Omega_z}$ into Eq. (A1) one obtains the basis truncation

$$\begin{aligned}\left(n_x + \frac{1}{2}\right) + \left(n_y + \frac{1}{2}\right)\frac{1}{P} + \left(n_z + \frac{1}{2}\right)\frac{1}{Q} \\ \leqslant (N_0 + 2)\left(\frac{1}{PQ}\right)^{1/3}.\end{aligned} \tag{A2}$$

In the first step, the truncation parameters P and Q, which are related to the deformations (β, γ), are initialized to P_0 and Q_0, respectively, through formulas based on a liquid drop parametrization of nuclear shape

$$\begin{aligned}P_0 &= \exp(-\alpha\sqrt{3}\sin\gamma), \\ Q_0 &= \exp\left[\alpha\left(\frac{3}{2}\cos\gamma - \frac{\sqrt{3}}{2}\sin\gamma\right)\right],\end{aligned} \tag{A3}$$

where $\alpha = \beta/(2\beta + 1)$.

Given $(N_0, P_0, \text{and } Q_0)$, one defines, using Eq. (A2), the maximal integer values reached by the numbers of quanta, namely N_x, N_y, and N_z. For N_x, one finds $N_x = E(\frac{N_0+2}{(P_0Q_0)^{1/3}} - \frac{P_0+Q_0}{2P_0Q_0})$, where $E(x)$ means the integer value of x.

In the second step, without altering the integer set (N_x, N_y, and N_z), a fine-tuning of P and Q values, starting from P_0 and Q_0, is performed to maximize the number of HO-basis states fulfilling Eq. (A2). This procedure leads to an increase of about ten units in the number of states initially considered in the basis.

For a given truncation of the basis (N_0, P, and Q), the parameter ω_0, defined as $\omega_0^3 = \omega_x\omega_y\omega_z$, is optimized through minimization of the HFB energy. Here ω_i is the HO frequency in each of the three spatial directions and the deformation parameters $p = \frac{\hbar\omega_x}{\hbar\omega_y}$ and $q = \frac{\hbar\omega_x}{\hbar\omega_z}$ are given explicitly by

$$\begin{aligned}p &= \exp(-\alpha\sqrt{3}\sin\gamma), \\ q &= \exp\left[\alpha\left(\frac{3}{2}\cos\gamma - \frac{\sqrt{3}}{2}\sin\gamma\right)\right].\end{aligned} \tag{A4}$$

This procedure avoids the use of gigantic HO-basis size for large deformations. In our calculations, each set of parameters are systematically optimized and/or calculated for each nucleus and each grid point on the (β, γ) plane.

[1] C. Détraz, D. Guillemaud, G. Huber, R. Klapisch, M. Langevin, F. Naulin, C. Thibault, L. C. Carraz, and F. Touchard, Phys. Rev. C **19**, 164 (1979).

[2] M. Bernas, Ph. Dessagne, M. Langevin, J. Payet, F. Pougheon, and P. Roussel, Phys. Lett. **B113**, 279 (1982).

[3] J. Dobaczewski, I. Hamamoto, W. Nazarewicz, and J. A. Sheikh, Phys. Rev. Lett. **72**, 981 (1994).

[4] S. Grévy, F. Negoita, I. Stefan, N. L. Achouri, J. C. Angélique, B. Bastin, R. Borcea, A. Buta, J. M. Daugas, F. De Oliveira, O. Giarmana, C. Jollet, B. Laurent, M. Lazar, E. Lienard, F. Marechal, J. Mrazek, D. Pantelica, Y. Penionzhkevich, S. Pietri, O. Sorlin, M. Stanoiu, C. Stodel, and M. G. St-Laurent, Eur. Phys. J. A **25**, s01, 111 (2005).

[5] E. Bouchez, I. Matea, W. Korten, F. Becker, B. Blank, C. Borcea, A. Buta, A. Emsallem, G. de France, J. Genevey, F. Hannachi, K. Hauschild, A. Hürstel, Y. Le Coz, M. Lewitowicz, R. Lucas, F. Negoita, F. de Oliveira Santos, D. Pantelica, J. Pinston, P. Rahkila, M. Rejmund, M. Stanoiu, and Ch. Theisen, Phys. Rev. Lett. **90**, 082502 (2003).

[6] R. G. Allatt, R. D. Page, M. Leino, T. Enqvist, K. Eskola, P. T. Greenlees, P. Jones, R. Julin, P. Kuusiniemi, W. H. Trzaska, and J. Uusitalo, Phys. Lett. **B437**, 29 (1998).

[7] O. Sorlin, S. Leenhardt, C. Donzaud, J. Duprat, F. Azaiez, F. Nowacki, H. Grawe, Zs. Dombrádi, F. Amorini, A. Astier, D. Baiborodin, M. Belleguic, C. Borcea, C. Bourgeois, D. M. Cullen, Z. Dlouhy, E. Dragulescu, M. Górska, S. Grévy, D. Guillemaud-Mueller, G. Hagemann, B. Herskind, J. Kiener, R. Lemmon, M. Lewitowicz, S. M. Lukyanov, P. Mayet, F. de Oliveira Santos, D. Pantalica, Yu.-E. Penionzhkevich, F. Pougheon, A. Poves, N. Redon, M. G. Saint-Laurent, J. A. Scarpaci, G. Sletten, M. Stanoiu, O. Tarasov, and Ch. Theisen, Phys. Rev. Lett. **88**, 092501 (2002).

[8] K. Langanke, J. Terasaki, F. Nowacki, D. J. Dean, and W. Nazarewicz, Phys. Rev. C **67**, 044314 (2003).

[9] S. Lunardi, S. M. Lenzi, F. Della Vedova, E. Farnea, A. Gadea, N. Mărginean, D. Bazzacco, S. Beghini, P. G. Bizzeti, A. M. Bizzeti-Sona, D. Bucurescu, L. Corradi, A. N. Deacon, G. de Angelis, E. Fioretto, S. J. Freeman, M. Ionescu-Bujor, A. Iordachescu, P. Mason, D. Mengoni, G. Montagnoli, D. R. Napoli, F. Nowacki, R. Orlandi, G. Pollarolo, F. Recchia, F. Scarlassara, J. F. Smith, A. M. Stefanini, S. Szilner, C. A. Ur, J. J. Valiente-Dobón, and B. J. Varley, Phys. Rev. C **76**, 034303 (2007).

[10] P. Adrich, A. M. Amthor, D. Bazin, M. D. Bowen, B. A. Brown, C. M. Campbell, J. M. Cook, A. Gade, D. Galaviz, T. Glasmacher, S. McDaniel, D. Miller, A. Obertelli, Y. Shimbara, K. P. Siwek, J. A. Tostevin, and D. Weisshaar, Phys. Rev. C **77**, 054306 (2008).

[11] O. Sorlin, C. Donzaud, F. Nowacki, J. C. Angelique, F. Azaiez, C. Bourgeois, V. Chiste, Z. Dlouhy, S. Grevy, D. Guillemaud-Mueller, F. Ibrahim, K.-L. Kratz, M. Lewitowicz, S. M. Lukyanov, J. Mrazek, Yu.-E. Penionzhkevich, F. de Oliveira Santos, B. Pfeiffer, F. Pougheon, A. Poves, M. G. Saint-Laurent, and M. Stanoiu, Eur. Phys. J. A **16**, 55 (2003).

[12] L. Gaudefroy, O. Sorlin, C. Donzaud, J. C. Angelique, F. Azaiez, C. Bourgeois, V. Chiste, Z. Dlouhy, S. Grévy, D. Guillemaud-Mueller, F. Ibrahim, K.-L. Kratz, M. Lewitowicz, S. M. Lukyanov, I. Matea, J. Mrazek, F. Nowacki, F. de Oliveira Santos, Yu.-E. Penionzhkevich, B. Pfeiffer, F. Pougheon, M. G. Saint-Laurent, and M. Stanoiu, Eur. Phys. J. A **23**, 41 (2005).

[13] O. B. Tarasov, D. J. Morrissey, A. M. Amthor, T. Baumann, D. Bazin, A. Gade, T. N. Ginter, M. Hausmann, N. Inabe, T. Kubo, A. Nettleton, J. Pereira, M. Portillo, B. M. Sherrill, A. Stolz, and M. Thoennessen, Phys. Rev. Lett. **102**, 142501 (2009).

[14] E. Clément, A. Görgen, W. Korten, E. Bouchez, A. Chatillon, J.-P. Delaroche, M. Girod, H. Goutte, A. Hürstel, Y. Le Coz, A. Obertelli, S. Péru, Ch. Theisen, J. N. Wilson, M. Zielińska, C. Andreoiu, F. Becker, P. A. Butler, J. M. Casandjian, W. N. Catford, T. Czosnyka, G. de France, J. Gerl, R.-D. Herzberg, J. Iwanicki, D. G. Jenkins, G. D. Jones, P. J. Napiorkowski, G. Sletten, and C. N. Timis, Phys. Rev. C **75**, 054313 (2007).

[15] J. Ljungvall, A. Görgen, M. Girod, J.-P. Delaroche, A. Dewald, C. Dossat, E. Farnea, W. Korten, B. Melon, R. Menegazzo, A. Obertelli, R. Orlandi, P. Petkov, T. Pissulla, S. Siem, R. P. Singh, J. Srebrny, Ch. Theisen, C. A. Ur, J. J. Valiente-Dobón, K. O. Zell, and M. Zielińska, Phys. Rev. Lett. **100**, 102502 (2008).

[16] J. Dudek, A. Goźdź, N. Schunck, and M. Miśkiewicz, Phys. Rev. Lett. **88**, 252502 (2002).

[17] J. Libert, M. Girod, and J.-P. Delaroche, Phys. Rev. C **60**, 054301 (1999).

[18] M. Girod and B. Grammaticos, Phys. Rev. C **27**, 2317 (1983).

[19] G. F. Bertsch, M. Girod, S. Hilaire, J.-P. Delaroche, H. Goutte, and S. Péru, Phys. Rev. Lett. **99**, 032502 (2007).

[20] A. Obertelli, S. Péru, J.-P. Delaroche, A. Gillibert, M. Girod, and H. Goutte, Phys. Rev. C **71**, 024304 (2005).

[21] S. Péru, M. Girod, and J. F. Berger, Eur. Phys. J. A **9**, 35 (2000).

[22] M. Girod, J.-P. Delaroche, A. Görgen, and A. Obertelli, Phys. Lett. **B676**, 39 (2009).

[23] J.-P. Delaroche, M. Girod, J. Libert, H. Goutte, S. Hilaire, S. Péru, N. Pillet, and G. F. Bertsch, submitted to Phys. Rev. C, arXiv:0910.2940v1.

[24] J. F. Berger, M. Girod, and D. Gogny, Nucl. Phys. **A502**, 85c (1989); Comput. Phys. Commun. **63**, 365 (1991).

[25] J. Dechargé and D. Gogny, Phys. Rev. C **21**, 1568 (1980).

[26] M. Bender, K. Bennaceur, T. Duguet, P.-H. Heenen, T. Lesinski, and J. Meyer, Phys. Rev. C **80**, 064302 (2009).

[27] S. Hilaire and M. Girod, Eur. Phys. J. A **33**, 237 (2007); http://www-phynu.cea.fr/HFB-Gogny_eng.htm.

[28] I. Hamamoto, H. Sagawa, and X. Z. Zhang, Phys. Rev. C **64**, 024313 (2001).

[29] M. Bender, P. Bonche, and P.-H. Heenen, Phys. Rev. C **74**, 024312 (2006).

[30] H. Oba and M. Hamamoto, Prog. Theor. Phys. **120**, 143 (2008).

[31] T. Kibédi and R. H. Spear, At. Data Nucl. Data Tables **80**, 35 (2002).

[32] Brookhaven database, http://www.nndc.bnl.gov.

[33] K. Langanke, D. J. Dean, and W. Nazarewicz, Nucl. Phys. **A728**, 109 (2003).

[34] Y. Sun, Y. C. Yang, H. L. Liu, K. Kaneko, M. Hasegawa, and T. Mizusaki, Phys. Rev. C **80**, 054306 (2009).

[35] R. Lecomte, S. Landsberger, P. Paradis, and S. Monaro, Phys. Rev. C **18**, 2801 (1978).

[36] W. G. Monahan and R. G. Arns, Phys. Rev. **184**, 1135 (1969).

[37] M. Didong, H. Müther, G. Goeke, and A. Faessler, Phys. Rev. C **14**, 1189 (1976).

[38] S. Iwasaki, T. Marumori, F. Sakata, and K. Takada, Prog. Theor. Phys. **56**, 1140 (1976).

[39] K. Takada and S. Tazaki, Nucl. Phys. **A395**, 165 (1983).